PHYSICAL REVIEW B **95**, 201403(R) (2017)

One-step synthesis of van der Waals heterostructures of graphene and two-dimensional superconducting α-Mo_2C

Jia-Bin Qiao,[1] Yue Gong,[2] Wei-Jie Zuo,[1] Yi-Cong Wei,[1] Dong-Lin Ma,[1] Hong Yang,[1] Ning Yang,[1] Kai-Yao Qiao,[1] Jin-An Shi,[2] Lin Gu,[2,3,4] and Lin He[1,*]

[1]*Center for Advanced Quantum Studies, Department of Physics, Beijing Normal University, Beijing 100875, China*
[2]*Beijing National Laboratory for Condensed Matter Physics, Institute of Physics, Chinese Academy of Sciences, Beijing 100190, China*
[3]*Collaborative Innovation Center of Quantum Matter, Beijing 100190, China*
[4]*School of Physical Sciences, University of Chinese Academy of Sciences, Beijing 100190, China*

(Received 21 March 2017; published 8 May 2017)

Assembling different two-dimensional (2D) crystals, covering a very broad range of properties, into van der Waals (vdW) heterostructures enables unprecedented possibilities for combining the best of different ingredients in one objective material. So far, metallic, semiconducting, and insulating 2D crystals have been used successfully in making functional vdW heterostructures with properties by design. Here, we expand 2D superconducting crystals as a building block of vdW hererostructures. One-step growth of large-scale high-quality vdW heterostructures of graphene and 2D superconducting α-Mo_2C by using chemical vapor deposition is reported. The superconductivity and its 2D nature of the heterostructures are characterized by our scanning tunneling microscopy measurements. This adds 2D superconductivity, the most attractive property of condensed matter physics, to vdW heterostructures.

DOI: 10.1103/PhysRevB.95.201403

Recently, van der Waals (vdW) heterostructures obtained via layer-by-layer stacking of different two-dimensional (2D) crystals [1–4] have attracted great interest [5–15]. The 2D crystals with various properties resemble atomic-scale Lego® blocks in building the ultimate vdW heterostructures. Interestingly, such artificial materials engineered with atomic accuracy exhibit properties distinct from their components, and, sometimes, they even show exotic phenomena that are beyond those already imaged [8–19]. For example, simply stacking graphene on top of an insulating hexagonal boron nitride (hBN) results in the emergence of topological currents in such a system [16,17]. Now, it is fair to say that scientists have already achieved great success by using 2D vdW heterostructures to realize materials with a variety of properties. However, 2D superconductivity, as the most attractive property of condensed matter physics, has not yet been achieved. Very recently, the newly discovered 2D superconductors [20–26] provide unprecedented opportunities to bring 2D superconductivity into vdW heterostructures. Via the proximity effect, the superconducting phase of superconductors can be introduced into nonsuperconducting crystals [27–32]. Therefore, it is reasonable to expect that the combination of 2D superconductors and other 2D crystals can lead to many extraordinary physical properties.

Here, we address this issue and report a feasible one-step growth of large-scale high-quality vdW heterostructures of graphene and 2D superconducting α-Mo_2C. Previously, graphene was grown successfully on groups IVB-VIB metal foils (including Mo foils) by chemical vapor deposition (CVD) [33–35]. In this Rapid Communication, we add a Cu foil on top of a Mo foil to directly grow graphene/α-Mo_2C heterostructures. Above 1085 °C (the melting point of Cu), the added Cu foil not only governs the diffusion process of Mo atoms to tune the chemical reaction rate, but also manipulates the growth mechanisms, thus realizing one-step growth of well-defined vdW heterostructures of graphene and α-Mo_2C.

Figure 1(a) shows schematic drawings of the growth mechanism for graphene/α-Mo_2C heterostructures. Above 1085 °C, Mo atoms diffuse into the melted Cu foil to form a Cu-Mo alloy. Then, we can control the final products by tuning the ratio λ of methane (CH_4) to hydrogen (H_2) during the growth process. At a low ratio ($\lambda \leqslant$ 1:500), we obtained well-defined 2D α-Mo_2C crystals due to the predominant "carbide growth" mechanism attributing to the large bonding strength between Mo and C atoms [23]. However, at a relatively high ratio ($\lambda >$ 1:500), there is a high level of C source and the onset of the "graphene growth" process is triggered. The added Cu foil plays a vital role in the formation of vdW heterostructures. It competes with the Mo component to capture C atoms for surface-catalytic graphene growth [36]. Assisted with the graphitic catalysis of preformed α-Mo_2C crystals, large-scale high-quality graphene grows on both the exposed Cu (Cu-Mo alloy) surface and α-Mo_2C crystals, thus generating 2D superconducting vdW heterostructures of graphene and α-Mo_2C, as shown in Fig. 1(b). The heterostructures usually show regular shapes, such as a triangle, rectangle, and hexagon, tailored by the underlying α-Mo_2C sheets [see Figs. 1(b)–1(f) and the Supplemental Material [37] for more details]. Importantly, it is convenient to control the dimension and thickness of the α-Mo_2C sheets in the heterostructures by changing the growth parameters, such as the ratio λ, the growth temperature and time, as well as the thickness of the Cu foil (see the Supplemental Material [37] for more details on the size adjustment). In our experiment, the size of the α-Mo_2C sheets in the heterostructures can be changed from a few micrometers to over 50 μm, and the thickness can be varied from a few nanometers to hundreds of nanometers.

Figure 1(g) shows a representative Raman spectrum of the obtained vdW heterostructures of graphene and α-Mo_2C transferred on a SiO_2/Si substrate (see the Methods section in the Supplemental Material [37] for more details). The three

*Corresponding author: helin@bnu.edu.cn

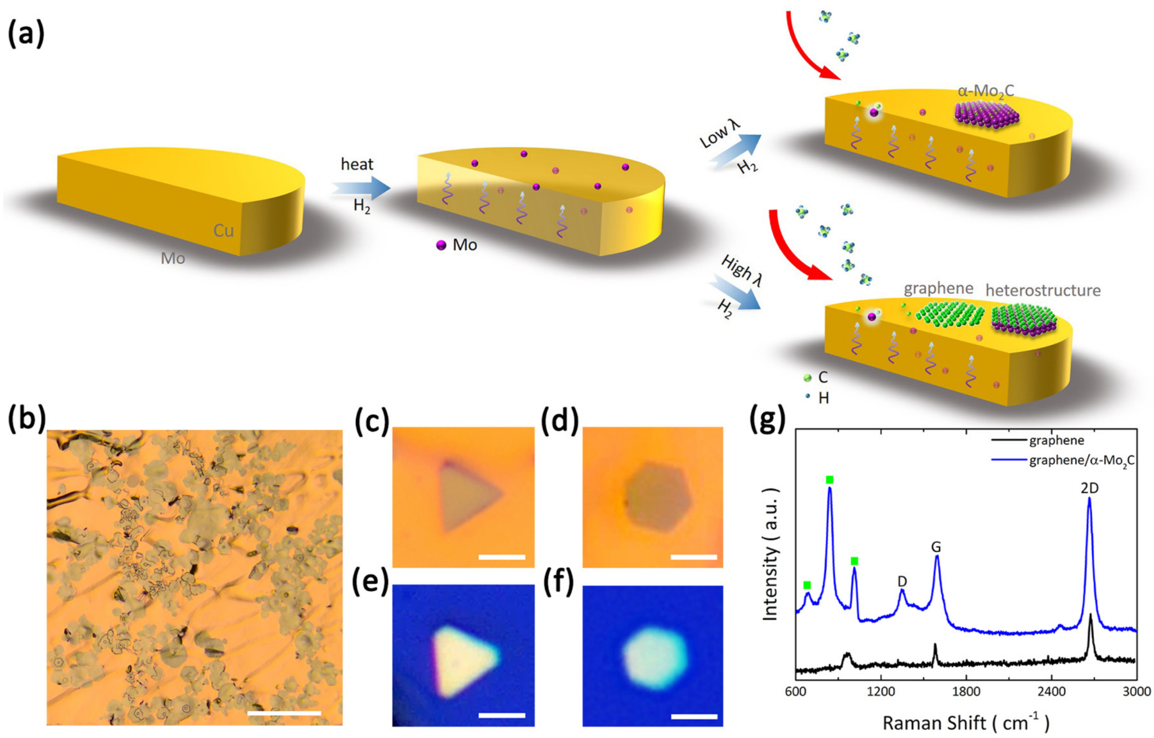

FIG. 1. Schematic of synthesis and optical characterizations of graphene/α-Mo_2C heterostructures. (a) Schematic illustration of the growth process for the heterostructures. A Cu foil is supported by a Mo substrate, and then Mo atoms start to diffuse across the liquid Cu at high temperatures with the flow of H_2. With a low ratio of CH_4 to H_2, C atoms are predominantly captured by Mo atoms (marked by luminous Mo and C atoms) and react into α-Mo_2C crystals. With a high ratio of CH_4 to H_2, we directly obtained graphene/α-Mo_2C heterostructures. (b) Optical image of graphene/α-Mo_2C heterostructures on a Cu (Cu-Mo alloy)/Mo substrate. Scale bar: 50 μm. Optical images exhibit as-grown [(c) and (d)] and transferred [(e) and (f)] regular polygon-shaped heterostructures on Cu and SiO_2/Si targets, respectively. All the scale bars are 5 μm. (g) Raman spectra for the transferred graphene sheets and graphene/α-Mo_2C heterostructures on SiO_2/Si targets. The green squares denote the Raman signals of α-Mo_2C, while the peak at low wave number ($\sim$970 cm^{-1}) in the graphene spectrum arises from the SiO_2/Si substrate.

peaks located at low wave numbers are characteristic signals of α-Mo_2C [38] and the G and $2D$ peaks of graphene [39] are also clearly observed in the Raman spectrum. In our experiment, we find that the $2D$ peak exhibits a symmetric single Lorentzian line shape and the intensity ratio of the G to $2D$ peaks falls in a range of 0.4–0.6. These features are the hallmarks of the Raman spectra of single-layer graphene, in accord with the favorable growth of monolayer graphene on transition-metal carbides (TMCs) [33]. Compared with the spectrum of the surrounding graphene sheet, a pronounced D peak emerges in the spectrum of graphene in the heterostructure [Fig. 1(g)], which may originate from the sp^3-hybridized defects caused by the strong bonding between the Mo and C atoms. The vdW heterostructures were further characterized by x-ray diffraction (XRD), energy dispersive x-ray spectra (EDS), atomic force microscopy (AFM), and x-ray photoelectron spectra (XPS) (see Figs. S10–S13 in the Supplemental Material [37] for more details). All these measurements demonstrated the creation of vdW heterostructures of graphene and 2D α-Mo_2C crystals.

The atomic structure of 2D vdW heterostructures has been investigated by high-resolution scanning transmission electron microscopy (HR-STEM), as visualized in Fig. 2. Figure 2(a) shows a low-magnification high-angle annular dark-field (HAADF)-STEM image of a hexagonal heterostructure. Figure 2(b) shows a selective area electron diffraction (SAED) pattern along the [100] zone axis of the heterostructure. The coexistence of two types of ED patterns from the α-Mo_2C and monolayer graphene confirms the formation of vdW heterostructures (see Fig. S16 in the Supplemental Material [37] for more details). According to the spatial distribution of the two sets of spots, the rotation orientation between α-Mo_2C (100) and the graphene lattices is extracted as $\sim 11^\circ$. Figure 2(c) shows the atomic-resolution HAADF-STEM image of the heterostructure. Despite the absence of a graphene lattice due to the insensibility on the light C atoms of the single-layer graphene sheet, the well-defined α-Mo_2C (100) lattices in an orthorhombic arrangement are clearly revealed, where six Mo atoms are arranged in a hexagonal close packed (hcp) structure and a C atom is located at the center of the hcp structure. Moreover, the HAADF-STEM cross-section image, as shown in Fig. 2(d), unveils the ABAB stacking of the Mo layers, which is consistent with the Mo lattice in the α-Mo_2C (010) surface. Obviously, all the STEM measurements validate the realization of graphene/α-Mo_2C heterostructures (see Figs. S13 and S15 in the Supplemental Material [37] for more details).

The well-defined graphene/α-Mo_2C vdW heterostructures provide an unprecedented platform to explore proximity-induced 2D superconductivity by using scanning tunneling

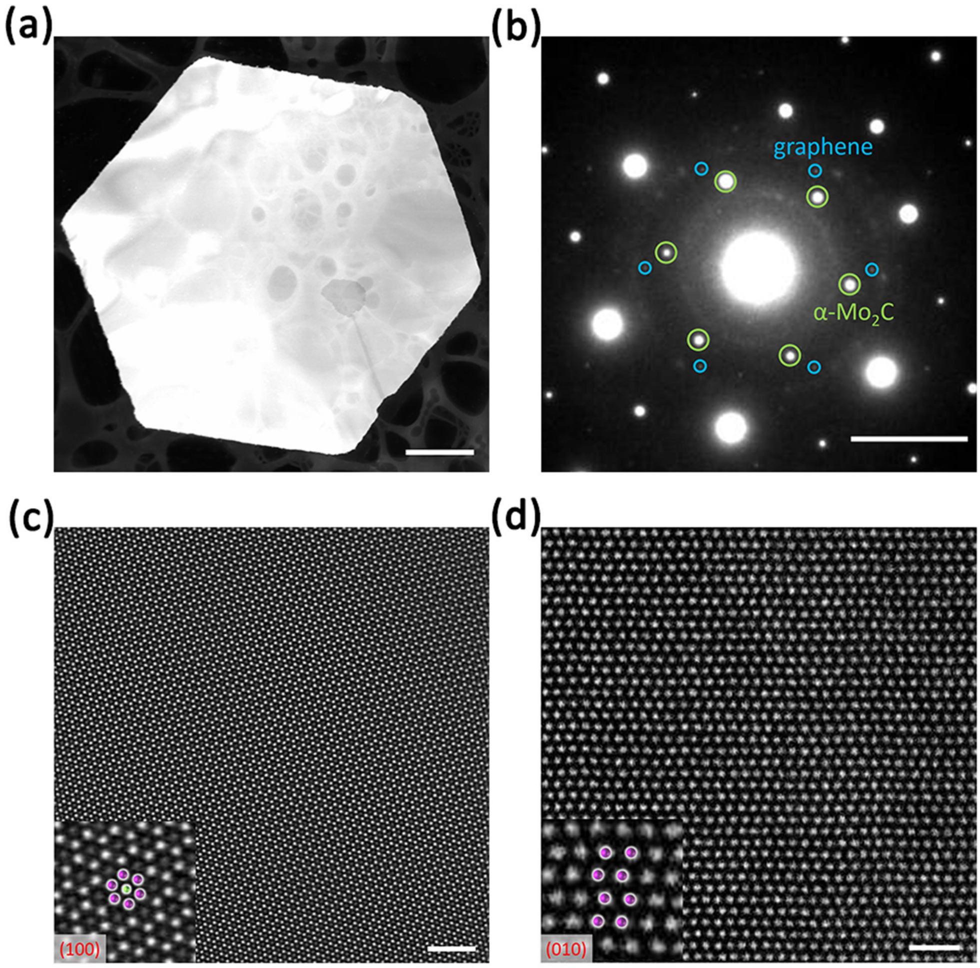

FIG. 2. Structural characterization of graphene/α-Mo_2C heterostructures. (a) Low-magnification HAADF-STEM image of the hexagonal graphene/α-Mo_2C heterostructures. Scale bar: 1 μm. (b) SAED pattern along the [100] zone axis, where some blue (green) spots belonging to graphene (α-Mo_2C) are circled. Scale bar: 5 nm^{-1}. The estimated lattice parameters of graphene and α-Mo_2C are $a_0 \sim 0.24$ nm and $b \sim 0.603$ nm, $c \sim 0.523$ nm, respectively. The twist angle between graphene and α-Mo_2C is extracted as $\sim 11^\circ$. Atomic-resolved HAADF-STEM images of the heterostructure surface parallel to the (100) facet (c) and cross section parallel to the (010) facet (d). This confirms the nature of the underlying α-Mo_2C crystals, where the center C atom (gray spot, marked by the green ball) is surrounded by six Mo atoms (white spots, marked by the purple balls) in a hcp arrangement in the (100) face and the Mo layers are arranged in ABAB-stacking form in the (010) face [insets in (c) and (d)], respectively. Both the scale bars are 1 nm.

microscopy/spectroscopy (STM/STS) [32,40]. Figure 3(a) shows a typical STM image of a monolayer graphene on the α-Mo_2C crystal (i.e., a graphene/α-Mo_2C heterostructure), which is characterized by peculiar patterns (moiré patterns) that are generated by the lattice mismatch between the surface of α-Mo_2C and graphene. The observed features differ from the surface topography of graphene grown on a Cu substrate (see Figs. S17 and S18 in the Supplemental Material [37]). Figure 3(b) shows an enlarged STM image of the heterostructure surface, where a hexagonal honeycomb lattice of monolayer graphene overlapping the moiré patterns is clearly observed. The coexistence of graphene and α-Mo_2C in the heterostructure is further confirmed by a fast Fourier transform (FFT) of the atomic-resolution STM image, as shown in Fig. 3(c). According to the FFT image, the rotated angle between the graphene and α-Mo_2C lattices in the heterostructure is about $(14 \pm 2)^\circ$, which is nearly equal to the results extracted from the SAED patterns. It is noticeable that there are six well-defined Bragg spots of the graphene reciprocal lattice, whereas only one pair of spots corresponding to the α-Mo_2C (100) reciprocal lattice are observed in the FFT of the STM image. This may possibly originate from the STM measurements as the STM predominantly probes the top graphene layer.

Figure 3(d) shows three representative tunneling spectra of the vdW heterostructure recorded at different temperatures. All the spectra exhibit V-shaped curves, as expected to be observed for the stable heterostructure where the graphene monolayer is supported by a metallic α-Mo_2C surface [41]. The Dirac point of graphene in the heterostructure is estimated to be at about -300 meV [see Fig. 3(d)]. Zooming in the spectrum measured at 400 mK, a superconducting gap appears at around E_F, as shown in Fig. 3(e). The superconducting gap in the spectrum can be well reproduced by the BCS Dynes fit [42] (see the Supplemental Material [37] for more details), directly revealing proximity-induced superconductivity in the graphene of the heterostructure.

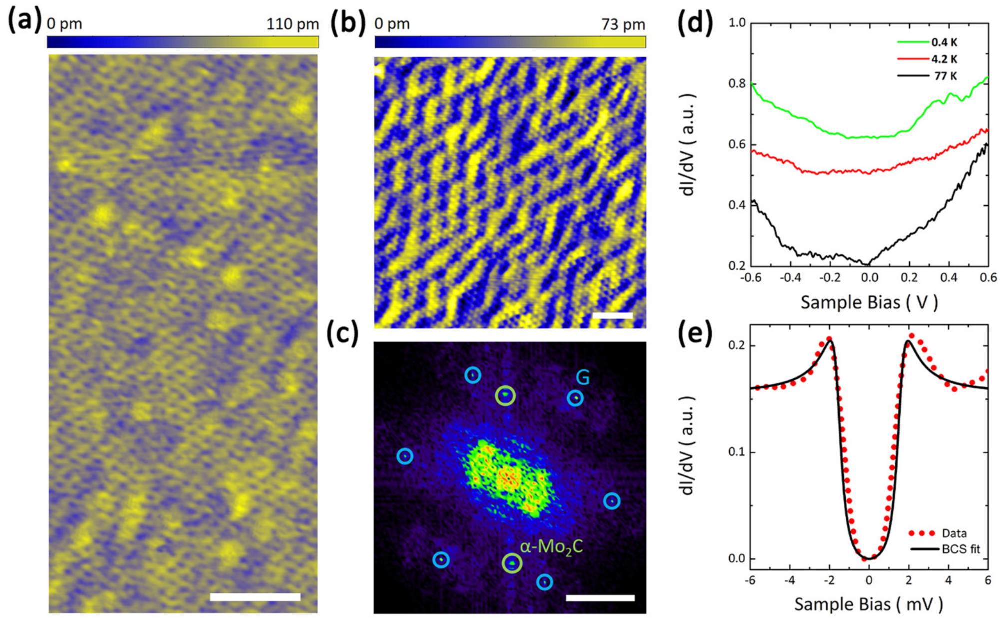

FIG. 3. Surface topography and superconducting gap of graphene/α-Mo_2C heterostructures. (a) Large-scale STM image of the heterostructures ($V_b = 1$ V, $I_S = 0.1$ nA). Scale bar: 5 nm. (b) Topographic closeup of the patterned surface ($V_b = 500$ mV, $I_S = 0.1$ nA). Scale bar: 1 nm. (c) Fast Fourier transform (FFT) image of the topography in (b). The outer six spots (marked by blue circles) and an inner pair of spots (marked by green circles) are the reciprocal lattice of graphene and α-Mo_2C, respectively. The derived lattice parameter of graphene is $a_0 \sim 0.24$ nm. The distance between the inner pair of spots is consistent with the crystalline interplanar spacing between the (002) and $(00\bar{2})$ faces of α-Mo_2C crystal ($\sim 7.68\ \mathrm{nm}^{-1}$), and one of the lattice constants is estimated as $c \sim 0.52$ nm. The twist angle between graphene and α-Mo_2C is measured as $\sim 14^\circ$. Scale bar: $3\ \mathrm{nm}^{-1}$. (d) STS spectra recorded in the patterned regions of the heterostructures at different temperatures. (e) A zooming-in dI/dV spectrum taken in the same region at 400 mK showing the superconducting gap (indicated by red dots). The black solid line is the theoretical BCS fitting with $\Delta = 1.58$ meV and $\Gamma = 0.4$ meV.

To further study the 2D superconductivity of the heterostructures, we carried out spectroscopic measurements at various temperatures and in the presence of perpendicular magnetic fields. In Fig. 4(a), we show the temperature evolution of the tunneling spectra measured at the same position of the heterostructure. The coherence peaks associated with the gaps are suppressed with increasing temperature, and finally vanish above $T \sim 3.9$ K. The superconducting gap of the heterostructure Δ, which is obtained by Dynes fitting of the spectra, as a function of temperature is shown in Fig. 4(c). The solid curve in Fig. 4(c) represents the best fit to the data by the BCS gap function. Based on the fitting, we extract the superconducting gap $\Delta(0)$ and T_c as 1.58 meV and 4.0 K, respectively, leading to a gap ratio $2\Delta(0)/k_BT_c$ of ~ 9.1. The ratio value is much larger than the one, $2\Delta(0)/k_BT_c \sim 3.53$, predicted by the BCS theory in the weak coupling regime [43], indicating a strong coupling mechanism in the system.

We also carried out spectroscopic measurements of the heterostructure in perpendicular magnetic fields. As shown in Fig. 4(b), the superconducting gap decreases with increasing the magnetic fields and disappears above ~ 200 mT at 0.4 K. Such a result matches well the predicted relationship between the gap and the applied fields [44], $\Delta(H)/\Delta(0) = \sqrt{1 - H/H_{c2}}$, as shown in Fig. 4(d).

Furthermore, the Ginzburg-Landau (GL) coherence length $\xi_{\mathrm{GL}}(0)$ is extracted as 38.5 nm from the general linearized GL relation $H_{c2}(T) = \Phi_0/2\pi\xi_{\mathrm{GL}}^2(0)(1 - T/T_c)$ (Φ_0 is the magnetic flux quantum). The value is larger than the thickness d_{SC} of the studied α-Mo_2C sheets, which are in the range of 10–30 nm (see Fig. S7 in the Supplemental Material [37]). This demonstrates the 2D superconducting behavior of the studied heterostructure. In our experiment, we found that the superconducting transition temperature T_c and the critical field $\mu_0 H_{c2}(T)$ of the heterostructures can be tuned by simply varying the thickness of the α-Mo_2C sheets in the heterostructures, as shown in Fig. 4(e). Therefore, because the thickness of the α-Mo_2C sheets is easy to control in the growth process, this provides a facile route to tune the superconductivity of the vdW heterostructures.

In conclusion, our experiments have turned on access to a one-step synthesis of large-scale high-quality vdW heterostructures of graphene and 2D superconducting α-Mo_2C. The well-defined superconducting heterostructures with flexible size adjustments not only offer an ideal system to further study the 2D superconducting properties of the artificial materials, but also open up the possibility to create designable high-quality superconducting heterostructure devices.

This work was supported by the National Natural Science Foundation of China (Grants No. 11674029, No. 11422430, No. 11374035, No. 51522212, No. 51421002, and No. 51672307), the National Basic Research Program of China (Grants No. 2014CB920903, No. 2013CBA01603, and No. 2014CB921002), the program for New Century Excellent Talents in University of the Ministry of Education of China (Grant

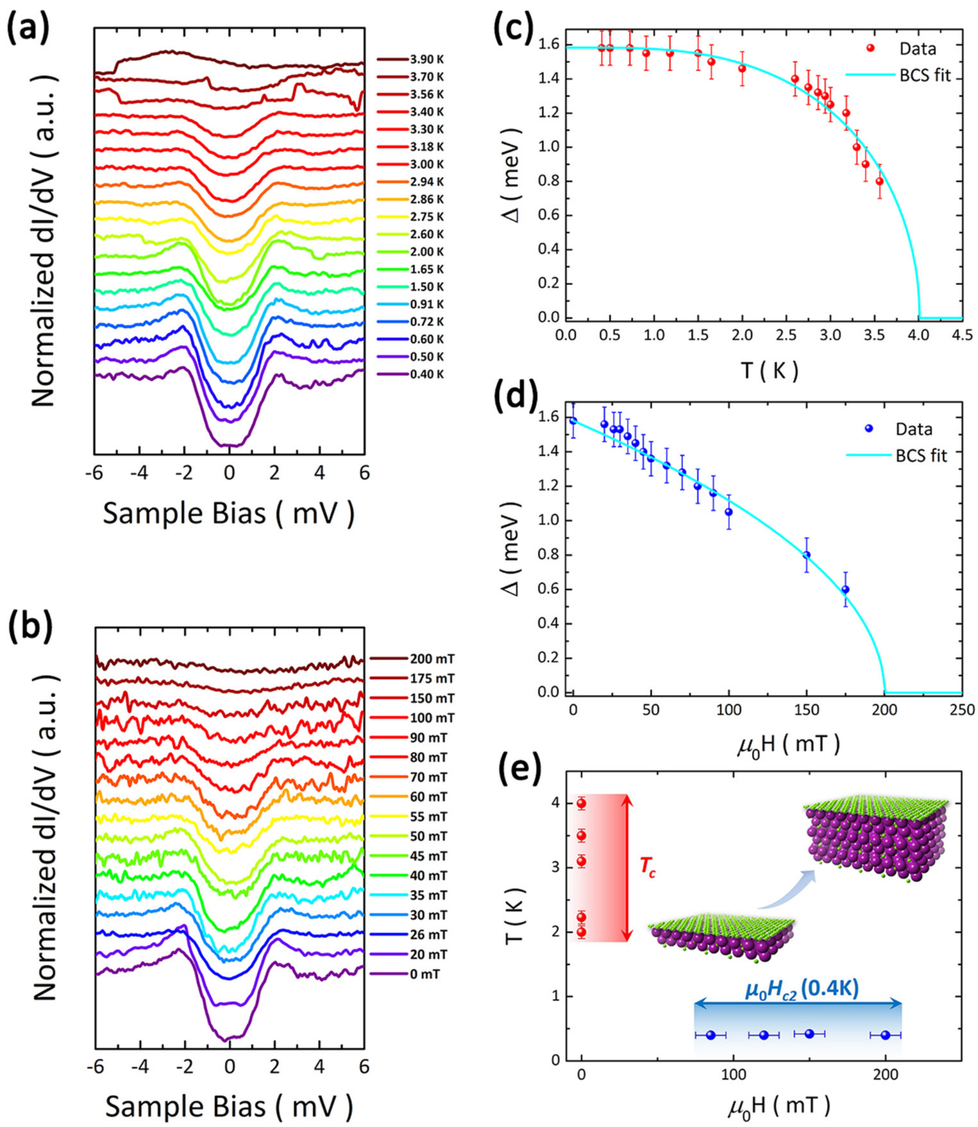

FIG. 4. Superconducting properties of the heterostructures. (a) Temperature evolution of superconducting tunneling spectra. The curves are offset on the y axis for clarity. a.u.: arbitrary units. (b) Normalized tunneling spectra as a function of applied magnetic fields. The curves are also offset on the y axis for clarity. (c) Temperature dependence of the superconducting gap. The measured $\Delta(T)$ is determined from a BCS fit to the tunneling spectra, and the light blue line is a theoretical result using the BCS gap function. (d) Magnetic field dependence of the superconducting gap. The measured $\Delta(T)$ is deduced from fitting the spectra in (b) to the BCS density of states, consistent with the relationship $\Delta(H)/\Delta(0) = \sqrt{1 - H/H_c}$. (e) Different superconducting transition temperatures and magnetic fields determined from the STS measurements. Red dots denote the variable T_c in the range of 2–4 K, while green and blue dots indicate the critical fields $\mu_0 H_{c2}(T)$, where $\mu_0 H_{c2}$ (0.4 K) varies from around 80 to 200 mT.

No. NCET-13-0054), the Strategic Priority Research Program of Chinese Academy of Sciences (Grant No. XDB07030200), and the Key Research Program of Frontier Sciences, CAS (Grant No. QYZDB-SSW-JSC035). L.H. also acknowledges support from the National Program for Support of Top-notch Young Professionals and support from “the Fundamental Research Funds for the Central Universities”.

J.-B.Q. and Y.G. contributed equally to this work.

[1] K. S. Novoselov, V. I. Fal’ko, L. Colombo, P. R. Gellert, M. G. Schwab, and K. Kim, A roadmap for graphene, Nature (London) **490**, 192 (2012).

[2] K. S. Novoselov, D. Jiang, F. Schedin, T. J. Booth, V. V. Khotkevich, S. V. Morozov, and A. K. Geim, Two-dimensional atomic crystals, Proc. Natl. Acad. Sci. USA **102**, 10451 (2005).

[3] S. Z. Butler *et al.*, Progress, challenges, and opportunities in two-dimensional materials beyond graphene, ACS Nano **7**, 2898 (2013).

[4] M. Xu, T. Liang, M. Shi, and H. Chen, Graphene-like two-dimensional materials, Chem. Rev. **113**, 3766 (2013).

[5] A. K. Geim and I. V. Grigorieva, van der Waals heterostructures, Nature (London) **499**, 419 (2013).

[6] K. S. Novoselov, A. Mishchenko, A. Carvalho, and A. H. Castro Neto, 2D materials and van der Waals heterostructures, Science **353**, 461 (2016).

[7] J. R. Wallbank *et al.*, Tuning the valley and chiral quantum state of Dirac electrons in van der Waals heterostructures, Science **353**, 575 (2016).

[8] M. Yankowitz, J. Xue, D. Cormode, J. D. Sanchez-Yamagishi, K. Watanabe, T. Taniguchi, P. Jarillo-Herrero, P. Jacquod, and B. J. LeRoy, Emergence of superlattice Dirac points in graphene on hexagonal boron nitride, Nat. Phys. **8**, 382 (2012).

[9] L. A. Ponomarenko *et al.*, Cloning of Dirac fermions in graphene superlattices, Nature (London) **497**, 594 (2013).

[10] C. R. Dean *et al.*, Hofstadter's butterfly and the fractal quantum Hall effect in moiré superlattices, Nature (London) **497**, 598 (2013).

[11] B. Hunt *et al.*, Massive Dirac fermions and Hofstadter butterfly in a van der Waals heterostructure, Science **340**, 1427 (2013).

[12] G. L. Yu *et al.*, Hierarchy of Hofstadter states and replica quantum Hall ferromagnetism in graphene superlattices, Nat. Phys. **10**, 525 (2014).

[13] C. R. Woods *et al.*, Commensurate-incommensurate transition in graphene on hexagonal boron nitride, Nat. Phys. **10**, 451 (2014).

[14] A. Avsar *et al.*, Spin-orbit proximity effect in graphene, Nat. Commun. **5**, 4875 (2014).

[15] Z. Wang, D. Ki, H. Chen, H. Berger, A. H. MacDonald, and A. F. Morpurgo, Strong interface-induced spin-orbit interaction in graphene on WS_2, Nat. Commun. **6**, 8339 (2015).

[16] R. V. Gorbachev *et al.*, Detecting topological currents in graphene superlattices, Science **346**, 448 (2014).

[17] M. Sui *et al.*, Gate-tunable topological valley transport in bilayer graphene, Nat. Phys. **11**, 1027 (2015).

[18] L. Ju *et al.*, Topological valley transport at bilayer graphene domain walls, Nature (London) **520**, 650 (2015).

[19] L. J. Yin, H. Jiang, J. B. Qiao, and L. He, Direct imaging of topological edge states at a bilayer graphene domain wall, Nat. Commun. **7**, 11760 (2016).

[20] Y. Saito, T. Nojima, and Y. Iwasa, Highly crystalline 2D superconductors, Nat. Rev. Mater. **2**, 16094 (2016).

[21] J. M. Lu, O. Zheliuk, I. Leermakers, N. F. Q. Yuan, U. Zeitler, K. T. Law, and J. T. Ye, Evidence for two-dimensional Ising superconductivity in gated MoS_2, Science **350**, 1353 (2015).

[22] M. M. Ugeda *et al.*, Characterization of collective ground states in single-layer $NbSe_2$, Nat. Phys. **12**, 92 (2016).

[23] C. Xu, L. Wang, Z. Liu, L. Chen, J. Guo, N. Kang, X. Ma, H. Cheng, and W. Ren, Large-area high-quality 2D ultrathin Mo_2C superconducting crystals, Nat. Mater. **14**, 1135 (2015).

[24] S. Ichinokura, K. Sugawara, A. Takayama, T. Takahashi, and S. Hasegawa, Superconducting calcium-intercalated bilayer graphene, ACS Nano **10**, 2761 (2016).

[25] Q. Wang *et al.*, Interface-induced high-temperature superconductivity in single unit-cell FeSe films on $SrTiO_3$, Chin. Phys. Lett. **29**, 037402 (2012).

[26] T. Uchihashi, Two-dimensional superconductors with atomic-scale thickness, Supercond. Sci. Technol. **30**, 013002 (2016).

[27] Y. Kozuka, M. Kim, C. Bell, B. G. Kim, Y. Hikita, and H. Y. Hwang, Two-dimensional normal-state quantum oscillations in a superconducting heterostructure, Nature (London) **462**, 487 (2009).

[28] M. X. Wang *et al.*, The coexistence of superconductivity and topological order in the Bi_2Se_3 thin films, Science **336**, 52 (2012).

[29] H. H. Sun *et al.*, Majorana Zero Mode Detected with Spin Selective Andreev Reflection in the Vortex of a Topological Superconductor, Phys. Rev. Lett. **116**, 257003 (2016).

[30] D. K. Efetov *et al.*, Specular interband Andreev reflections at van der Waals interfaces between graphene and $NbSe_2$, Nat. Phys. **12**, 328 (2016).

[31] M. B. Shalom *et al.*, Quantum oscillations of the critical current and high-field superconducting proximity in ballistic graphene, Nat. Phys. **12**, 318 (2016).

[32] C. Tonnoir, A. Kimouche, J. Coraux, L. Magaud, B. Delsol, B. Gilles, and C. Chapelier, Induced Superconductivity in Graphene Grown on Rhenium, Phys. Rev. Lett. **111**, 246805 (2013).

[33] Z. Zou, L. Fu, X. Song, Y. Zhang, and Z. Liu, Carbide-forming groups IVB-VIB metals: A new territory in the periodic table for CVD growth of graphene, Nano Lett. **14**, 3832 (2014).

[34] B. Dai, L. Fu, Z. Zou, M. Wang, H. Xu, S. Wang, and Z. Liu, Rational design of a binary metal alloy for chemical vapour deposition growth of uniform single-layer graphene, Nat. Commun. **2**, 522 (2011).

[35] J. B. Qiao, H. Jiang, H. Liu, H. Yang, N. Yang, K. Y. Qiao, and L. He, Bound states in nanoscale graphene quantum dots in a continuous graphene sheet, Phys. Rev. B **95**, 081409(R) (2017).

[36] X. Li *et al.*, Large-area synthesis of high-quality and uniform graphene films on copper foils, Science **324**, 1312 (2009).

[37] See Supplemental Material at http://link.aps.org/supplemental/10.1103/PhysRevB.95.201403 for methods, more charaterizations, and details of the analysis.

[38] T. C. Xiao, A. P. E. York, H. Al-Megren, C. V. Williams, H. T. Wang, and M. L. H. Green, Preparation and characterisation of bimetallic cobalt and molybdenum carbides, J. Catal. **202**, 100 (2001).

[39] A. C. Ferrari *et al.*, Raman Spectrum of Graphene and Graphene Layers, Phys. Rev. Lett. **97**, 187401 (2006).

[40] F. D. Natterer, J. Ha, H. Baek, D. Zhang, W. G. Cullen, N. B. Zhitenev, Y. Kuk, and J. A. Stroscio, Scanning tunneling spectroscopy of proximity superconductivity in epitaxial multilayer graphene, Phys. Rev. B **93**, 045406 (2016).

[41] J. Politi, F. Vines, J. A. Rodriguezc, and F. Illas, Atomic and electronic structure of molybdenum carbide phases: Bulk and low Miller-index surfaces, Phys. Chem. Chem. Phys. **15**, 12617 (2013).

[42] R. C. Dynes, V. Narayanamurti, and J. P. Garno, Direct Measurement of Quasiparticle-Lifetime Broadening in a Strong-Coupled Superconductor, Phys. Rev. Lett. **41**, 1509 (1978).

[43] J. Bardeen, L. N. Cooper, and J. R. Schrieffer, Theory of superconductivity, Phys. Rev. **108**, 1175 (1957).

[44] N. Levy, T. Zhang, J. Ha, F. Sharifi, A. A. Talin, Y. Kuk, and J. A. Stroscio, Experimental Evidence for s-Wave Pairing Symmetry in Superconducting $Cu_xBi_2Se_3$ Single Crystals Using a Scanning Tunneling Microscope, Phys. Rev. Lett. **110**, 117001 (2013).